Supplementary Material

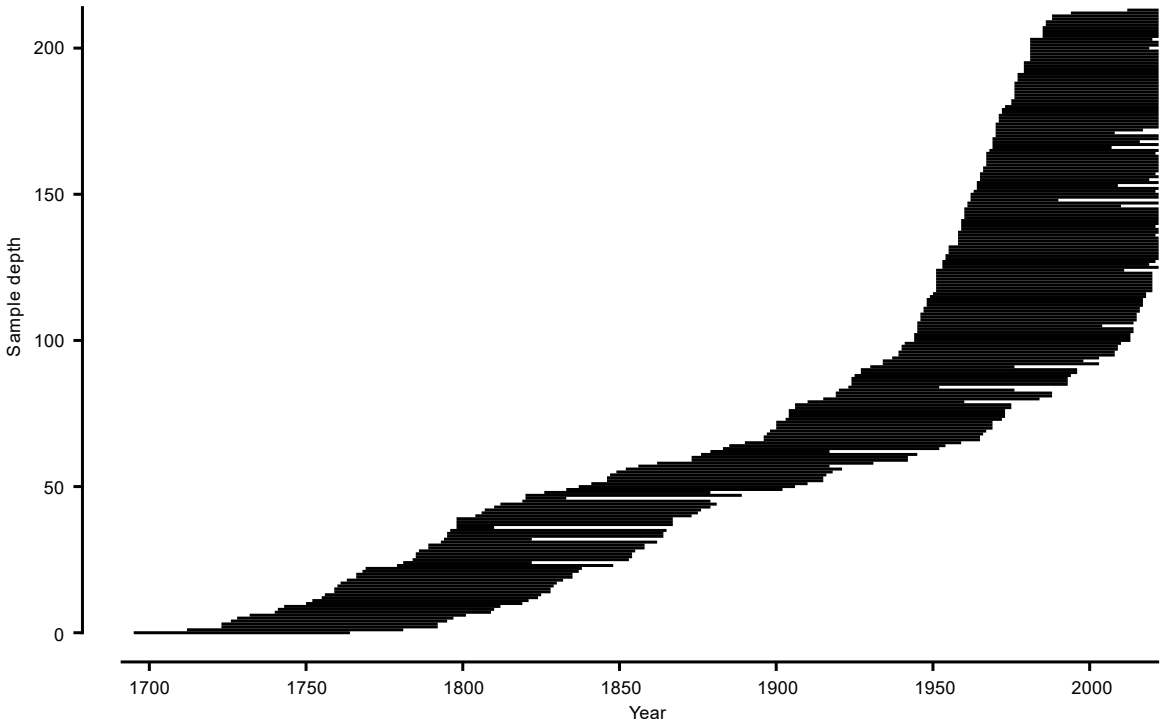

Fig. S 1: Segment length and sample replication used for RCS detrending.

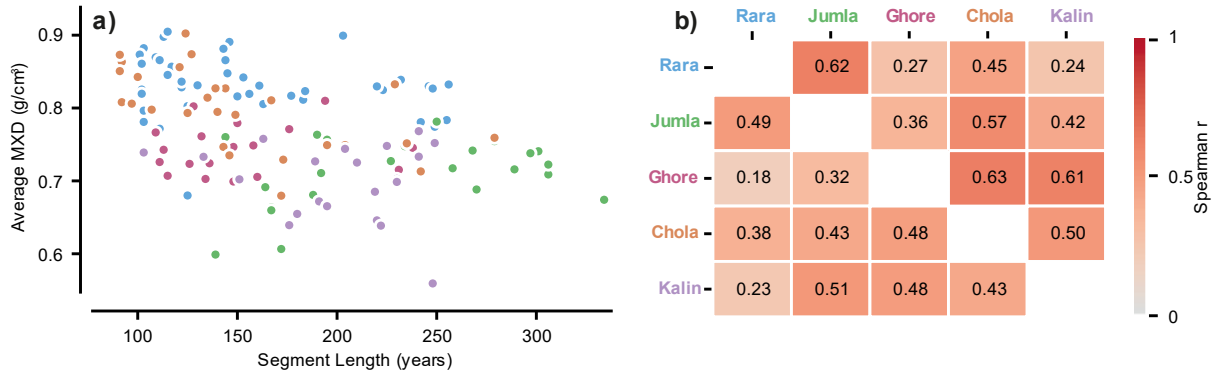

Fig. S 2: a) Average maximum latewood density (MXD) for the raw series against the segment length and b) inter-site correlations of detrended chronologies for their common period (1803–1979): lower triangle shows Spearman correlations, and upper triangle shows the corresponding correlations based on first differences

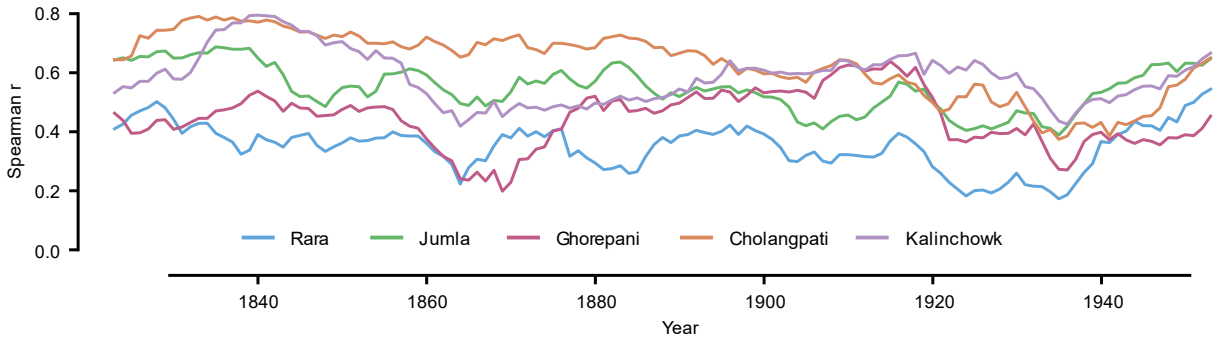

Fig. S 3: running correlations (51 year centered windows) between each site and the mean of the four remaining sites.

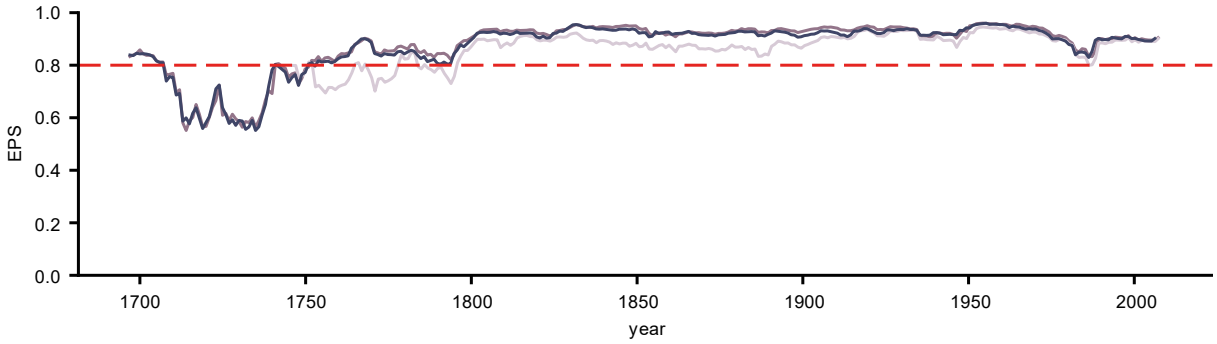

Fig. S 4: 30-year running EPS values for the mean-of-five, mean-of-four and mean-of-three chronologies.

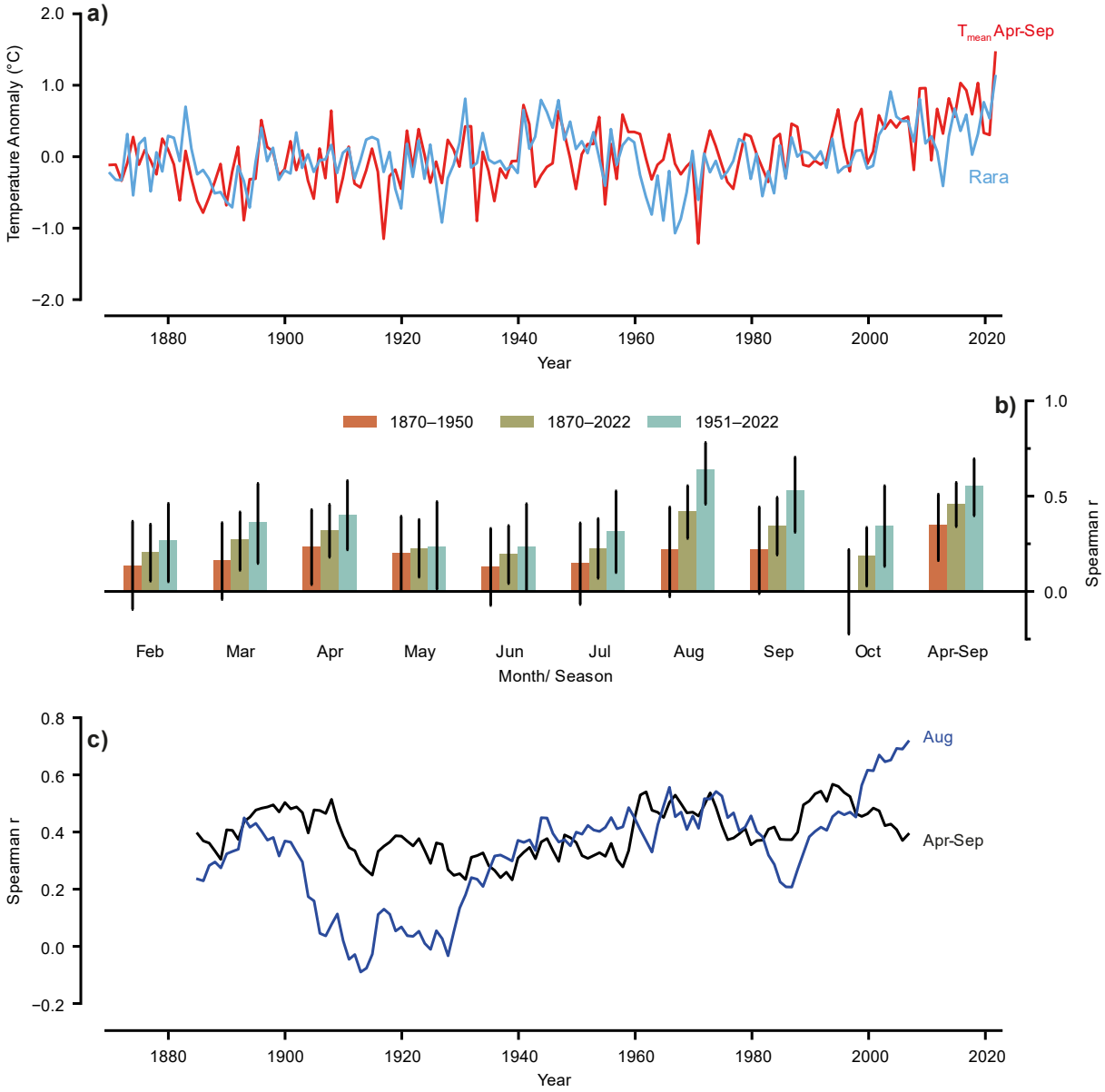

Fig. S 5: a) Rara Negex chronology scaled to April–September T_{mean} over 1900–1990; b) Seasonal correlations between T_{mean} and the Rara single-site chronology for three periods: 1870–1950, 1870-2022 and 1951–2022; c) Running correlations (31 year centered window) between August T_{mean} and the Rara single site chronology, and April–September T_{mean} and the Rara single-site chronology

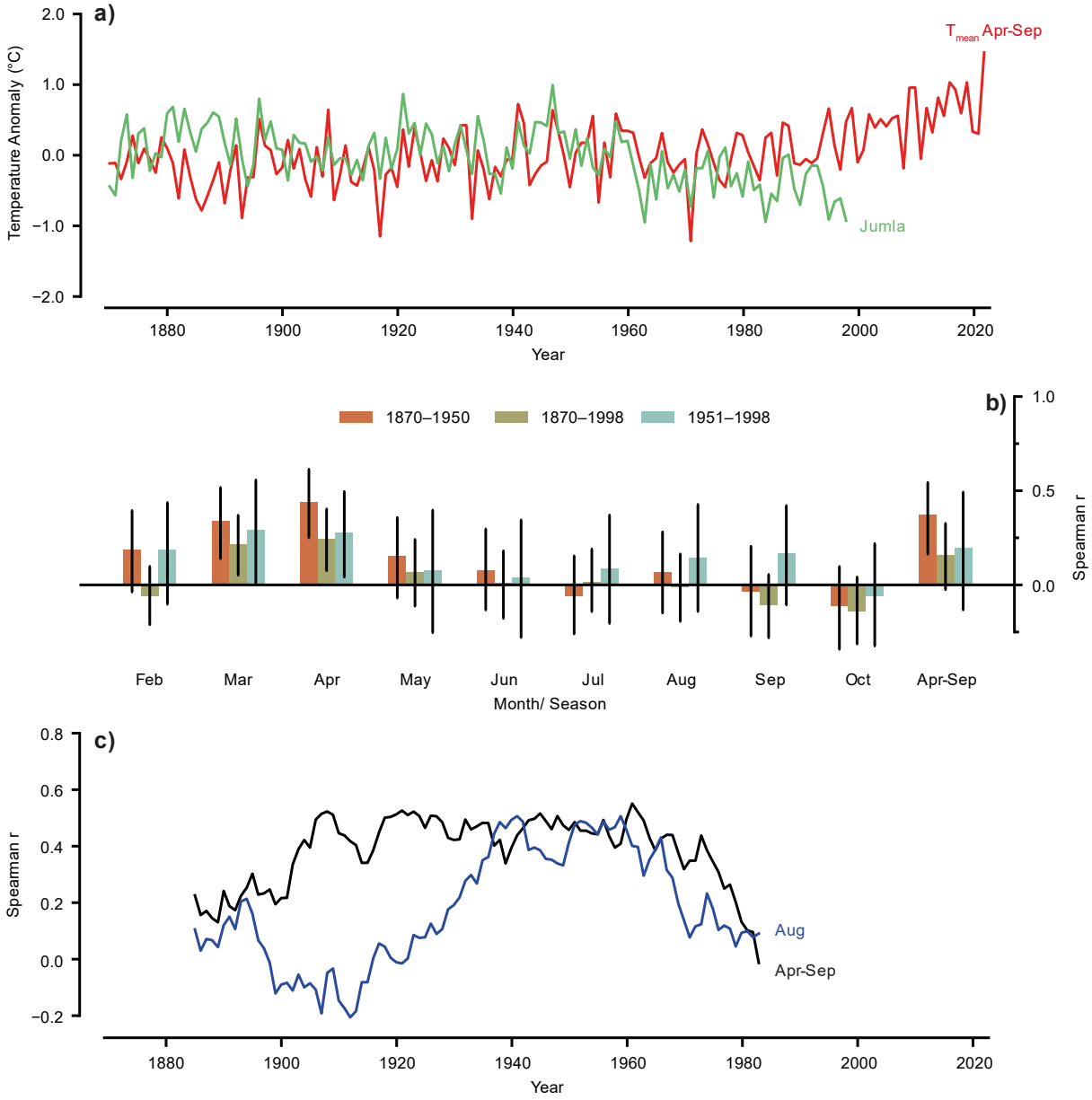

Fig. S 6: a) Jumla Negex chronology scaled to April–September T_{mean} over 1900–1990; b) Seasonal correlations between T_{mean} and the Jumla single-site chronology for three periods: 1870–1950, 1870-2022 and 1951–2022; c) Running correlations (31 year centered window) between August T_{mean} and the Jumla single site chronology, and April–September T_{mean} and the Jumla single-site chronology

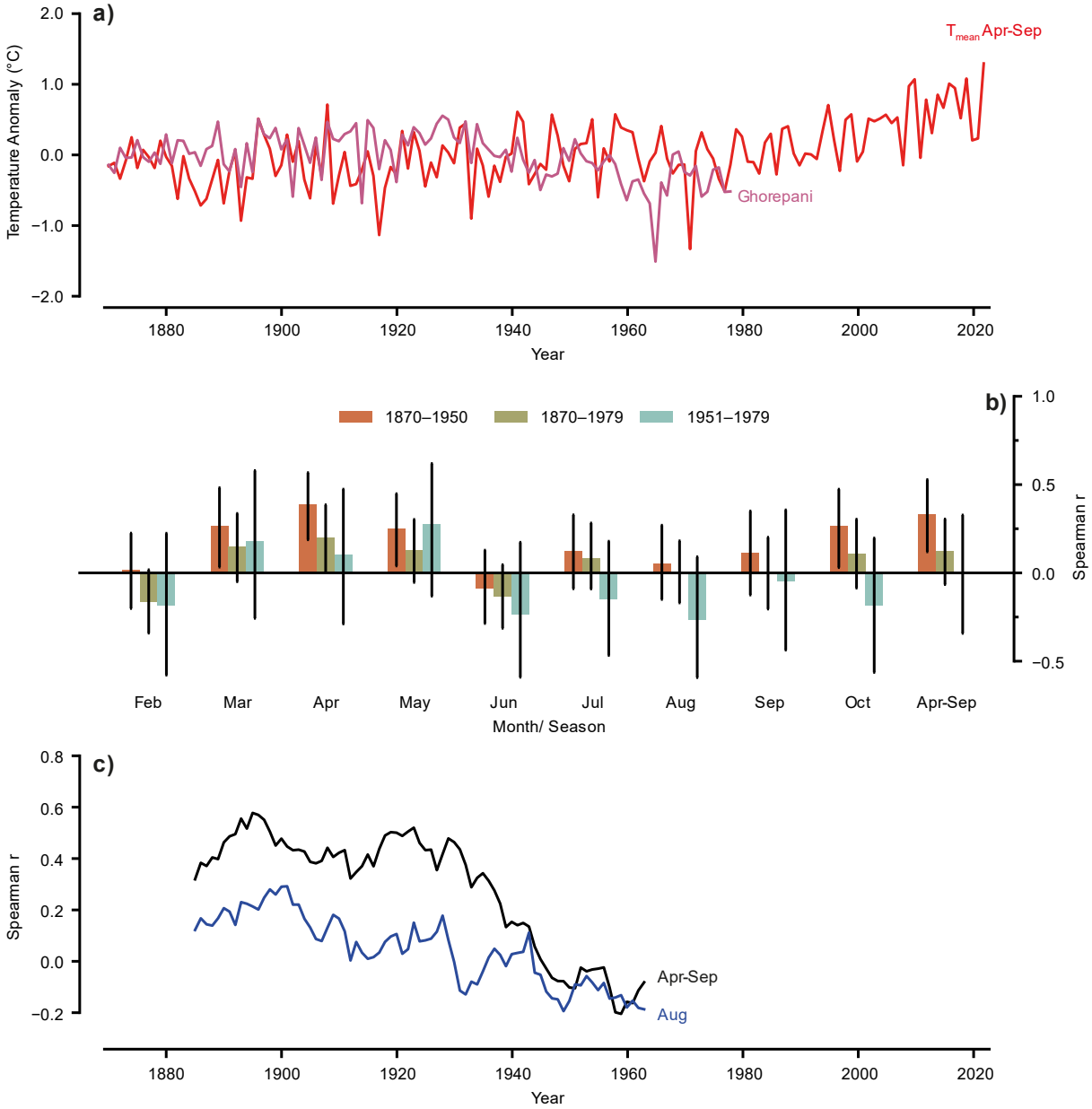

Fig. S 7: a) Ghorepani Negex chronology scaled to April–September T_{mean} over 1900–1990; b) Seasonal correlations between T_{mean} and the Ghorepani single-site chronology for three periods: 1870–1950, 1870-2022 and 1951–2022; c) Running correlations (31 year centered window) between August T_{mean} and the Ghorepani single site chronology, and April–September T_{mean} and the Ghorepani single-site chronology

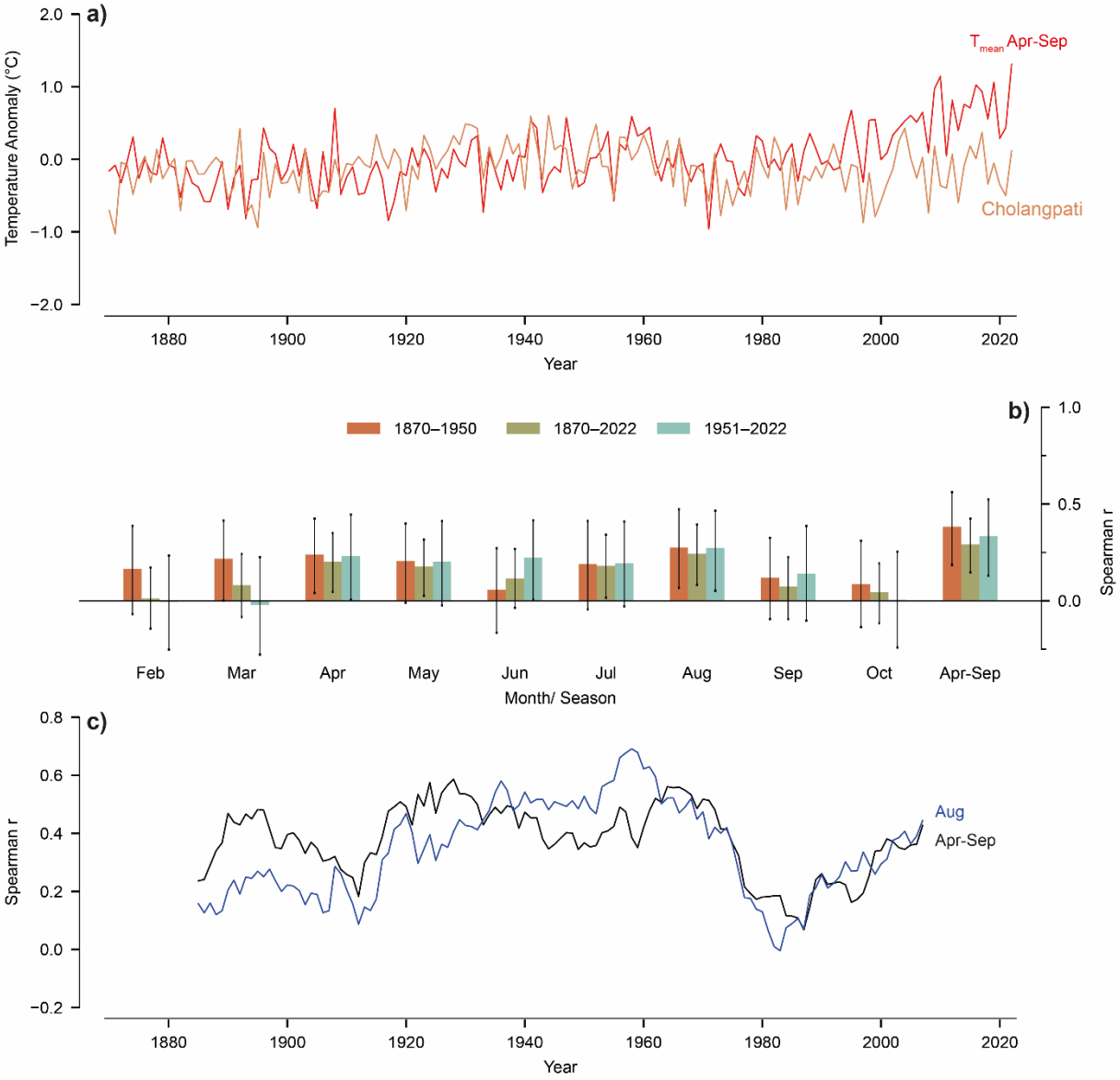

Fig. S 8: a) Cholangpati Negex chronology scaled to April–September T_{mean} over 1900–1990; b) Seasonal correlations between T_{mean} and the Cholanpati single-site chronology for three periods: 1870–1950, 1870-2022 and 1951–2022; c) Running correlations (31 year centered window) between August T_{mean} and the Cholangpati single site chronology, and April–September T_{mean} and the Cholangpati single-site chronology

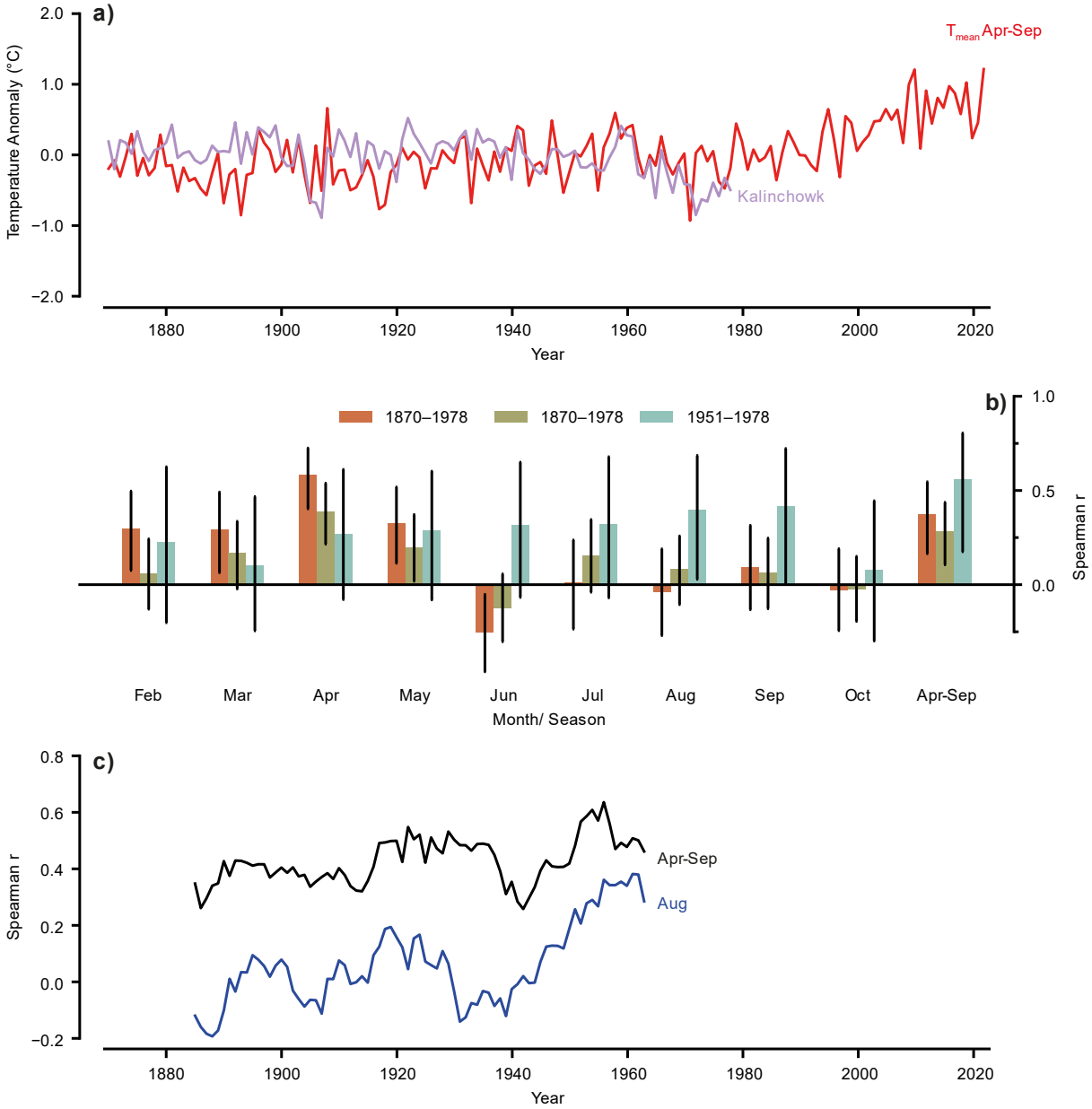

Fig. S 9: a) Kalinchowk Negex chronology scaled to April–September T_{mean} over 1900–1990; b) Seasonal correlations between T_{mean} and the Kalinchowk single-site chronology for three periods: 1870–1950, 1870-2022 and 1951–2022; c) Running correlations (31 year centered window) between August T_{mean} and the Kalinchowk single site chronology, and April–September T_{mean} and the Kalinchowk single-site chronology

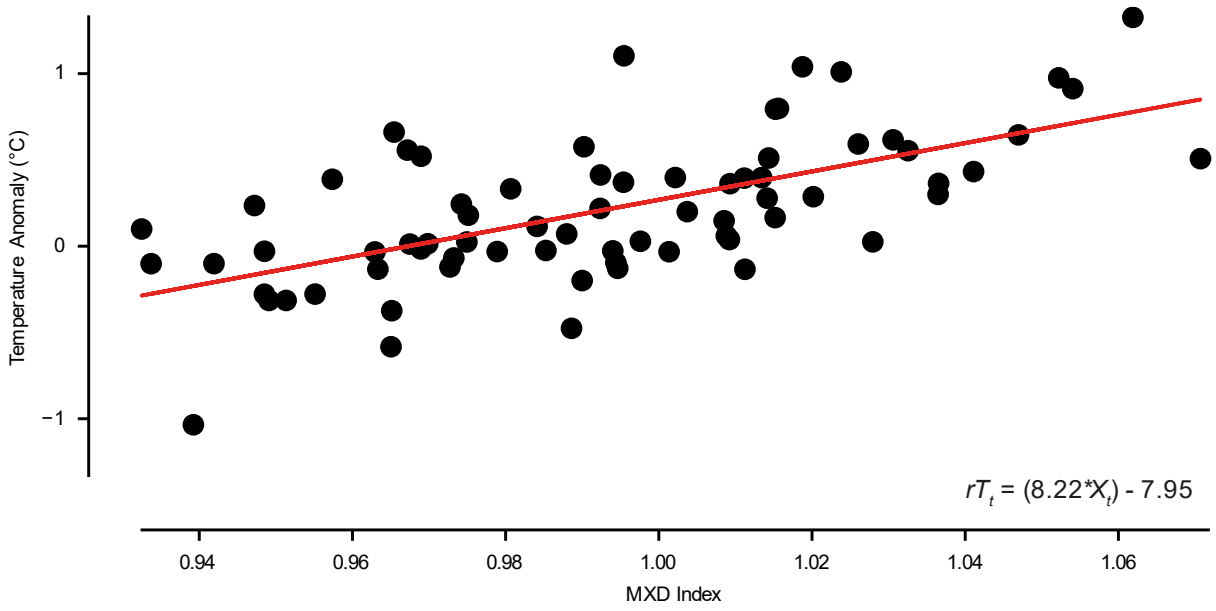

Fig. S 10: Scatter plot showing the relationship between MXD values and observed Apr-Sep T_{mean} during the full calibration period (1951–2022), with the transfer function fitted as a regression line.

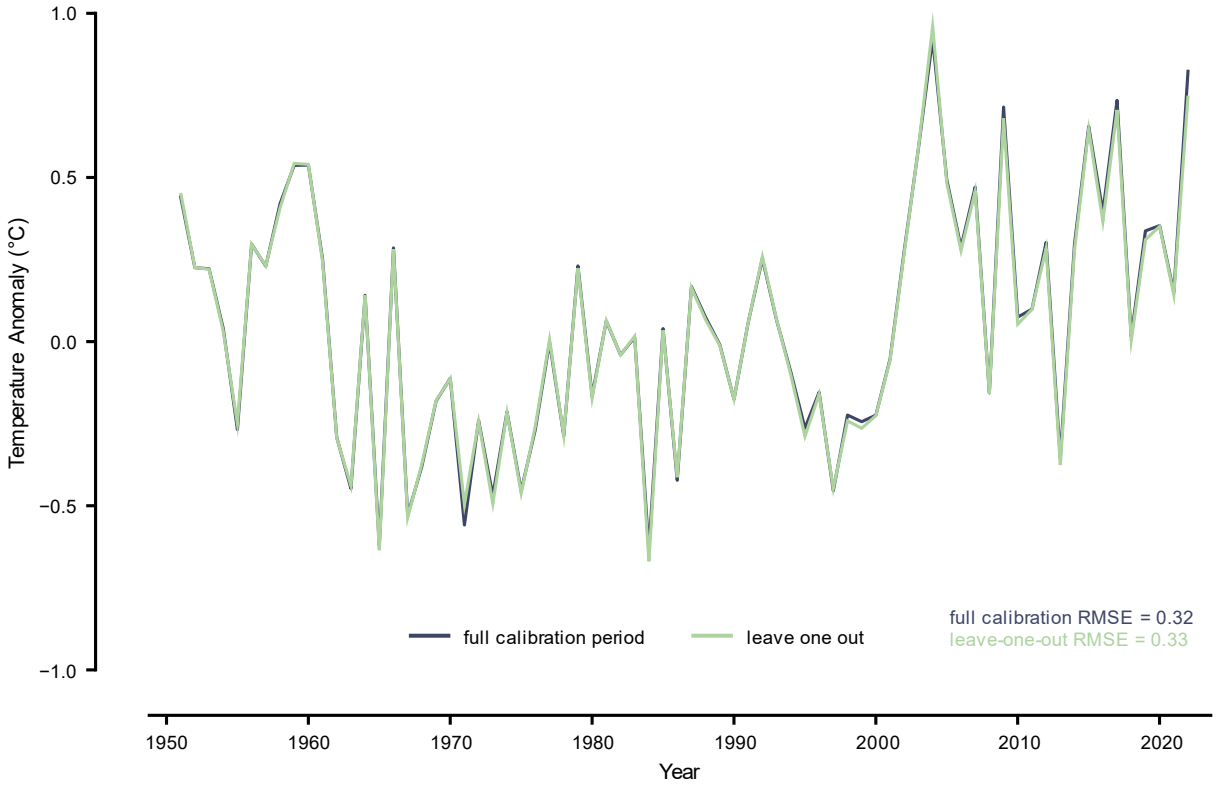

Fig. S 11: Leave-one-out cross calibration (green) and full calibration period (blue) for the mean-of-four composite chronology.

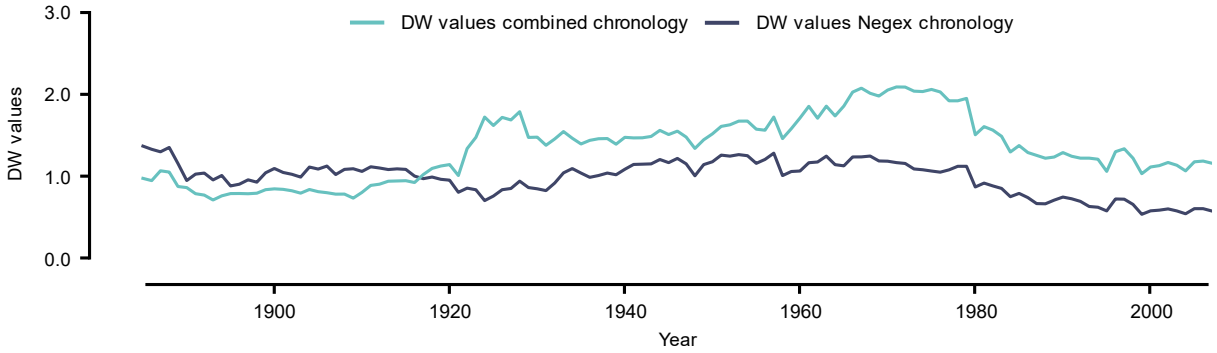

Fig. S 12: 31-year running Durbin Watson (DW) values for the mean-of-four composite chronology (dark blue) and the combined RCS Negex chronology (turquoise).

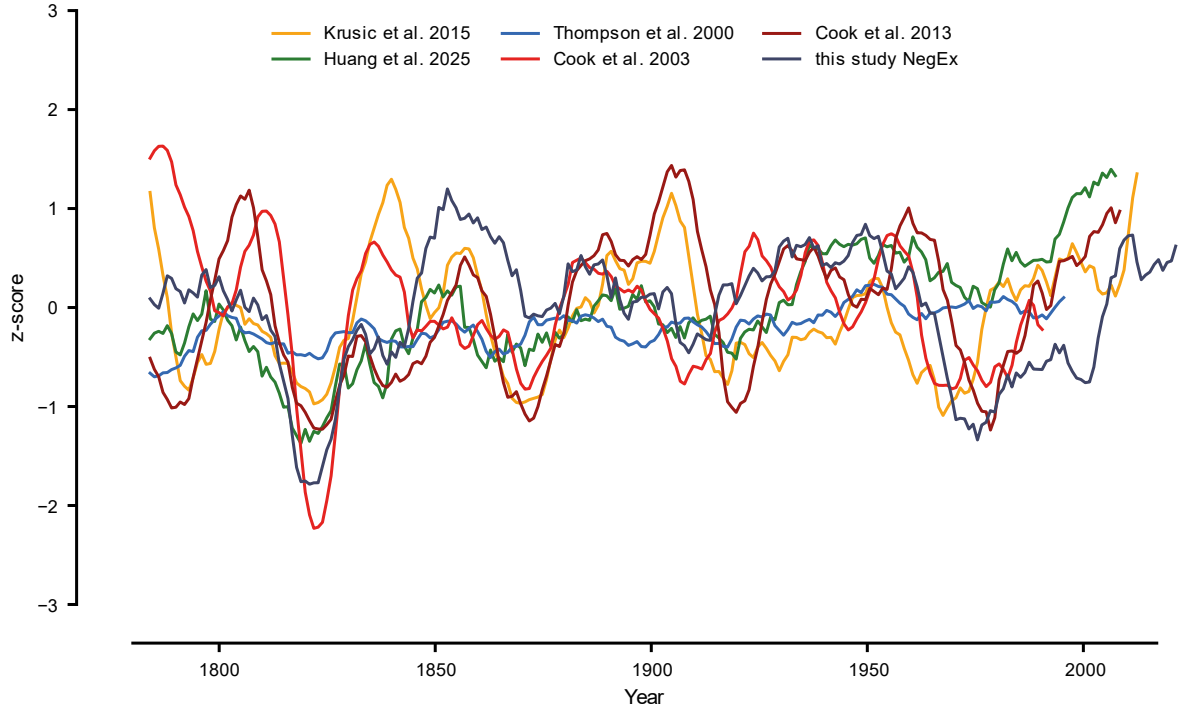

Fig. S 13: Running 10-year means (end year) of different reconstructions from the Himalayas and the Tibetan Plateau and the mean-of-four composite reconstruction from this study.

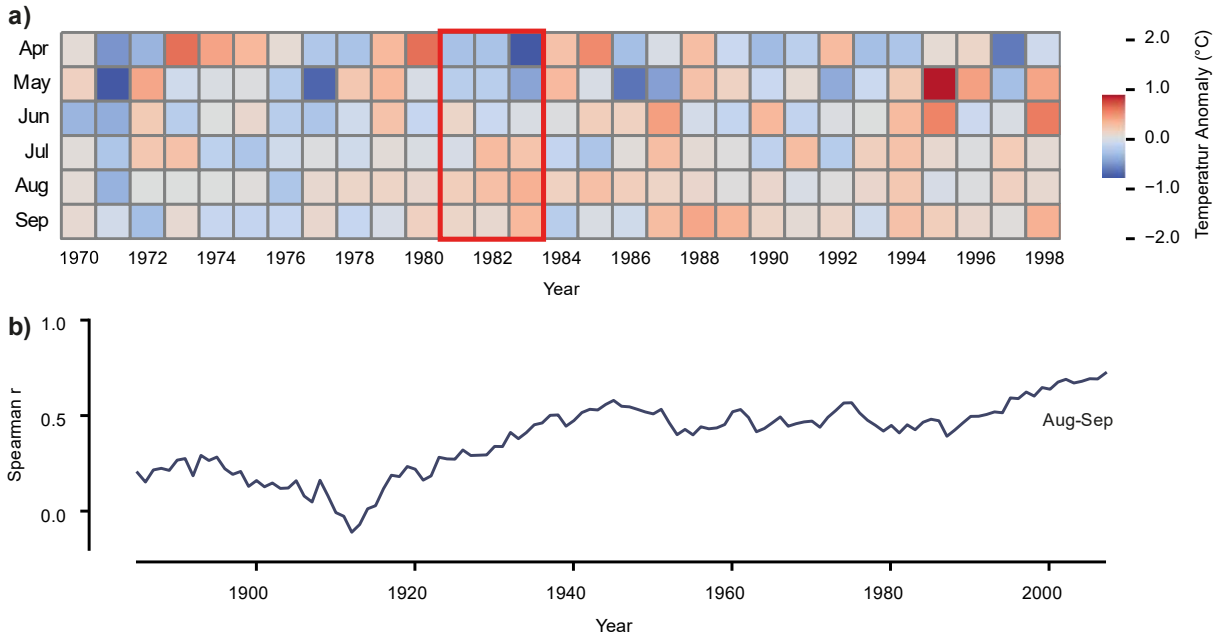

Fig. S 14 a) Monthly temperature anomalies for 1970–1998, red box marking three consecutive cold springs followed by a warmer summer; b) Running correlations between mean-of-four chronology and August–September T_{mean}.

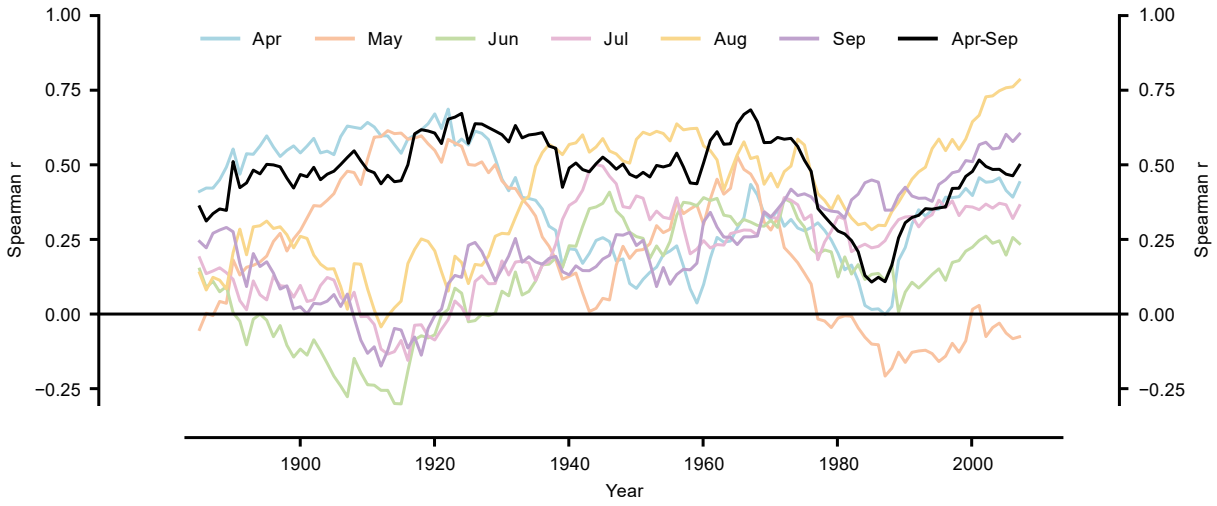

Fig. S 15: 31-year running correlations between the mean-of-four composite chronology and single month T_{mean} (colors) and Apr-Sep T_{mean} (black) over the period 1870–2022.

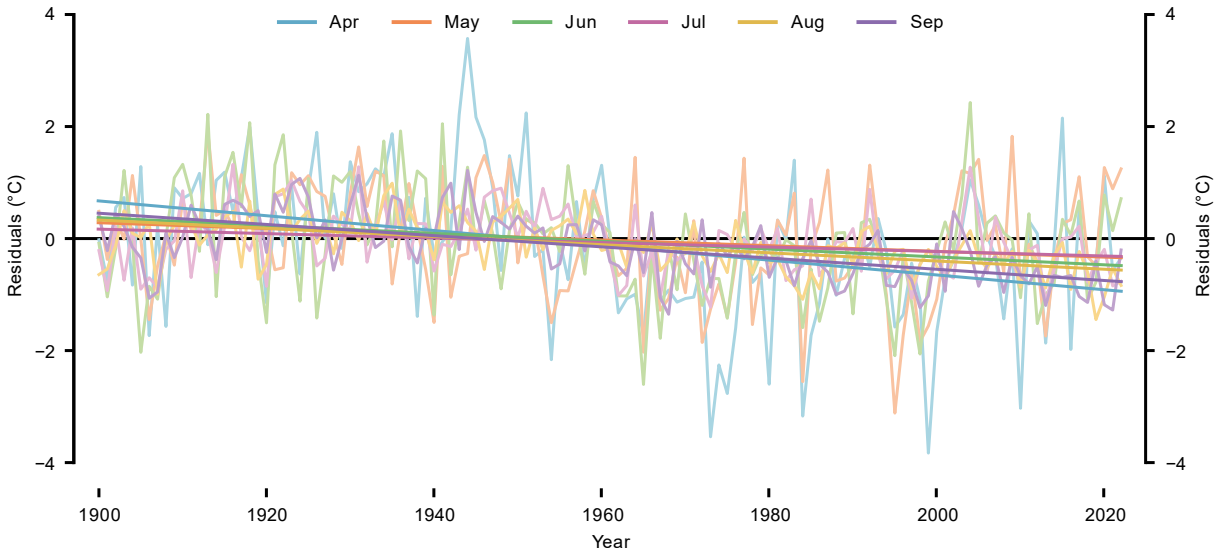

Fig. S 16: Residuals between the mean-of-four chronology scaled to single month temperatures (1900-1990) and the corresponding single month temperatures. Straight lines show regression-based trend lines.

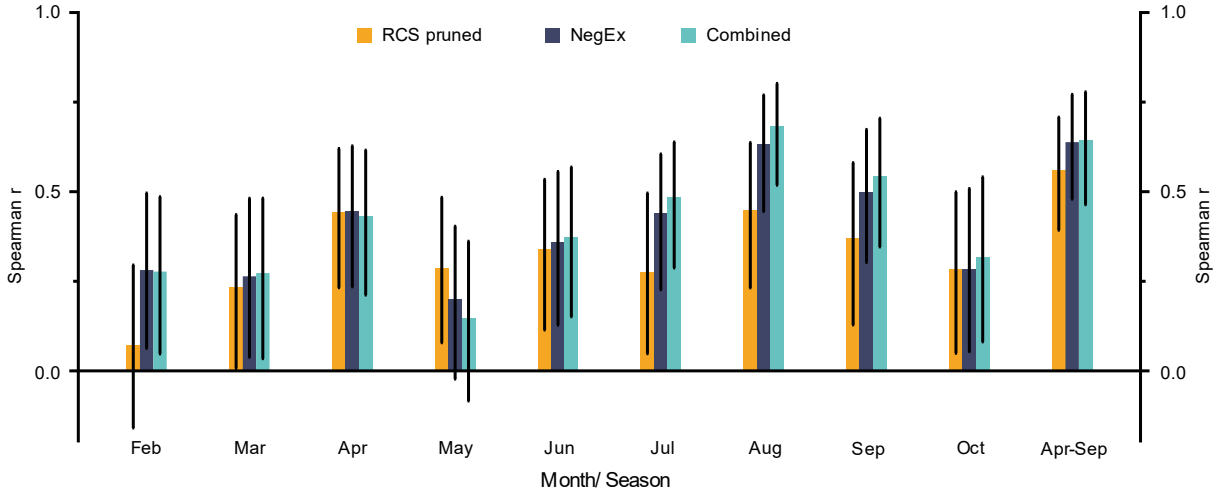

Fig. S 17: Seasonal correlations between T_{mean} and the three detrendings: pruned RCS, NegEx, and the combined chronology.

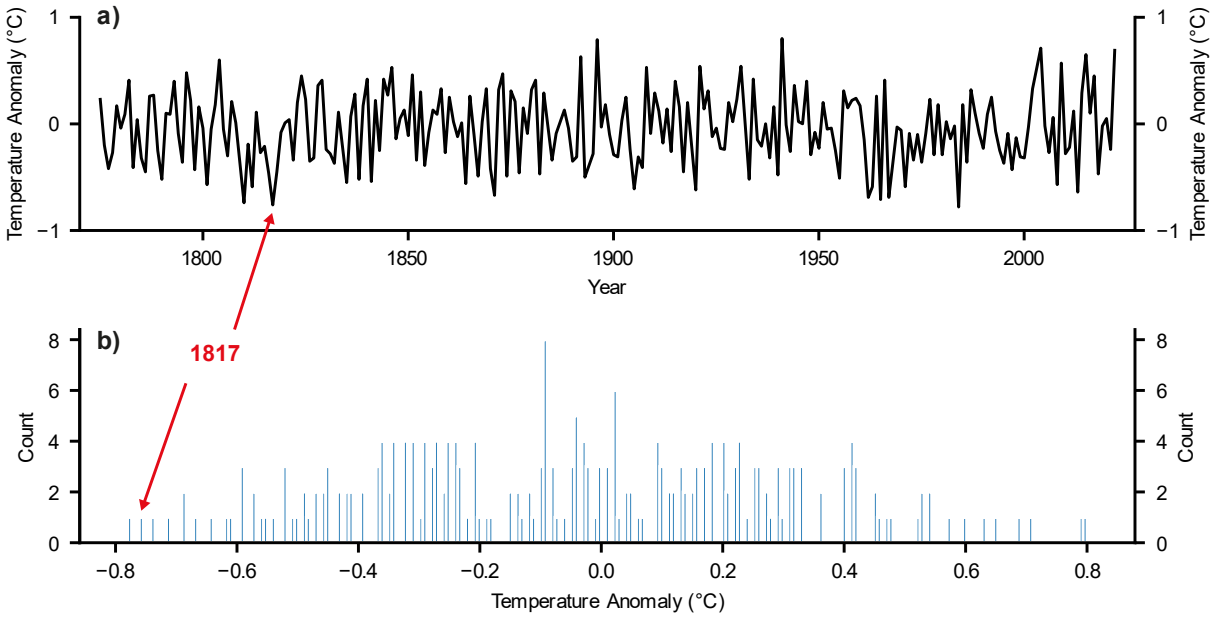

Fig. S 18: a) Pre-whitened version of the NegEx chronology and b) Empirical frequency distribution of the chronology values.

Table S 1. Calibration statistics for the combined NegEx and pruned RCS Apr–Sep T_{mean} reconstruction (CRE = calibration reduction of error, CE coefficient of efficiency, RE = reduction of error

	Calibration		Verification		
Period	r^2	CRE	r^2	RE	CE
1951–2022	0.45	0.67	–	–	–
1951–1975	0.45	0.59	0.38	0.52	0.27
1976–2022	0.38	0.66	0.45	0.62	0.30